CrystEngComm

Accepted Manuscript

ROYAL SOCIETY OF CHEMISTRY

www.rsc.org/crystengcomm

Effects of ethylenediamine in the formation of macro-, micro, and nanostructures based on $[W^{VI}(Cat)_2O_2]^{2-}$

Ganghuo Pan[a] Xiaoming Lu*[ab] Kai Li[a] Minghai Shen[a] Jing Zhao[a]

Department of Chemistry, Capital Normal University, China, Beijing 100048

b State Key Laboratory of Structural Chemistry, Fujian Institute of Research on the Structure of Matter, Chinese Academy of Sciences, Fuzhou, Fujian 350002, China.

E-mail: lu-xiaoming@126.com

Abstract:

We synthesized yellow needle-shaped crystal **1** with one-dimensional chain-like quantum motif consisted of $(NH_3CH_2CH_2NH_3)_{0.5}(NH_3CH_2CH_2NH_2)[(Cat)_2W^{VI}(O)_2]\cdot(NH_2CH_2CH_2NH_2)$ (1), and red-bulk crystal **2** with multi-tubular quantum unit composed of $(NH_3CH_2CH_2NH_2)_2[(Cat)_2W^{VI}(O)_2]$ (2) with a slight change in protonated degree of ethylenediamine. By grinding and ultra-sonication, crystal **1** disintegrated into nanowires with diameter of about 18nm and lengths of 300-1000nm, and crystal **2** disassembled into nano-tubules with diameter of 15-18nm and lengths of 450-550nm. Form the quantum motifs in crystal lattices we found that the quantum motifs in crystal lattices are the template of the nanostructures i.e the quantum-chains induced the formation of the nanowires and the quantum-tubules led to the production of the nano-tubules. To seek the mechanism that delicate change of ethylenediamine can cause great transformations of nanostructures, taking the nano-pipe-bundles (rather than nanowires) prepared from crystal 3 as comparison, although crystal 3 and 1 have the same crystal parameters, they have different ethylenediamine i.e. $(NH_3CH_2CH_2NH_2)_2[(Cat)_2W^{VI}(O)_2]\cdot(NH_2CH_2CH_2NH_2)$ (3). As everyone knows, the electrostatic attraction of the bi-protonated cation $(NH_3CH_2CH_2NH_3)^{2+}$ to anion $[(Cat)_2W^{VI}(O)_2]^{2-}$ is stronger than neutral molecule $NH_2CH_2CH_2NH_2$. And the multi-$[(Cat)_2W^{VI}(O)_2]^{2-}$-based chains were induced to split into a variety of cracks by different protonated ethylenediamine, therefore manufactured different nano-architectures. This paper revealed that slight changes in the protonation of ethylenediamine can induce nanostructures assembled by $[(Cat)_2W^{VI}(O)_2]^{2-}$ to form a variety of morphologies and sizes. And we recommended a new idea and method to prepare quite different tungsten organic hybrids nanostructures by changing the protonation degree of ethylenediamine.

Introduction

Tungsten-based nanostructures pioneered by R. Tenneet al.[1] play an important role in catalysis,[2–4] tribology,[5–7] sensors,[8–10] etc. Preparations of tungsten-based nano-architectures mostly involve conventional methods and, in some circumstances, a combination of them. Typically, these techniques may include bio-template,[11] carburization,[12–14] chemical vapor deposition,[15–17] combustion,[18,19] epitaxy,[20] mechanical grinding,[21] micelle,[22,23] microwave,[24–26] plasma,[27–29] precipation.[30,31] The preparation methods of nano-materials can be generally categorized into two approaches: top-down (concerning the dispersion of bulk materials, followed by aggregation process) and bottom-up (i.e. to construct nano-species using atoms or molecules). However, the preparation of nano-species which can be controlled and repeated still need to be overcome and the formation mechanisms are not yet clarified. In previous paper, [32-39] we have designed a series of bulk crystal constructed by Mo- and W-based coordinated-structures. Furthermore, by milling and ultrasonication, we disassemble the single crystals into nanowires, nanoparticles, nano-tubules and nano-ribbons. Especially, we have prepared different nanostructures from bulk crystals consisted of $[(Cat)_2W^{VI}(O)_2]^{2-}$ that combined with protonated ethylenediamine, protonated 1,2-propanediamine, and protonated 1,3-propanediamine, respectively.[40] And we demonstrated that the morphologies of the nano-aggregates in the paper are associated with the quantum motifs in their crystal lattices; for instance, the quantum-spots induced the formation of nanoparticles, quantum-wire lured the production of nano-ribbons, etc. To study further, two tungsten containing single crystals $[NH_3CH_2CH_2NH_2]_2[W^{VI}O_2(O_2C_6H_4)_2]$ (1) and $[NH_3CH_2CH2NH_3]_{0.5}[NH_3CH_2CH_2NH_2][W^{VI}O_2(O_2C_6H_4)_2]\cdot[NH_2CH_2CH_2NH_2]$ (2) were synthesized successfully, of which the differences between the two complexes are only the degree of protonation of ethylenediamine. By grinding and ultra-sonication, we disassembled the bulk single crystal 1 into micro-wires, and the diameter of the micro-wires is a few nanometers, the length is hundreds of nanometers. Mass of micro-wires gathered into nano-wire-bundles, the diameter is dozens of nanometers and length is hundreds of nanometers. Also the bulk crystal 2 disassembled and reassembled into nano-tubules, the diameter is hundreds of nano-meters and the length is about several microns. Interesting found, the slight change of the protonation for ethylenediamine resulted in nanostructures changed greatly.

Experimental section

1. Materials and Measurements. All reagents were directly obtained from commercial suppliers and were analytical grade without further purification. All manipulations were carried out in the laboratory atmosphere. Single crystal structure determination was performed on a Bruker APEXII area detector device with Mo/Ka and Cu/Ka radiation (λ = 0.71073 and 1.54178 Å) by the $\Phi-\omega$ scan method. The transmission electron microscopy (TEM) experiments were recorded on a Hitachi 7650 electron microscope. The scanning electron microscopy (SEM) experiments were recorded on a Hitachi SU8010 electron microscope. The IR spectra were recorded with KBr pellets on a Bruker EQUINOX 55 FT-spectrometer in the range of 4000-400 cm^{-1}; The ^{1}HNMR spectra were characterized on a Varian VNMRS 600MHz; the Elemental Analysis were recorded on a PE 2400Ⅱ;Redox stability characterized by a computer-controlled electrochemical analyzer (CHI 600E, Chenhua, China). The UV-vis absorption experiments were recorded on a Hitachi UV2550 instrument.

2. Synthesis of Bulk Single Crystals.

Preparation of crystal 1 and 2

25 g $Na_2WO_4\cdot 2H_2O$ was dissolved in 250 ml H_2O, HCl (1: 1) was used to adjust the solution PH to 3.5, then 8 g

$(C_4H_9)_4NBr$ was added at room temperature. One hour later, the solution was filtrated and the white powder of $[(n\text{-}Bu)_4N]_4W_{10}O_{32}$ was obtained, 50℃ of vacuum drying about one day (yield: 62%). Then, 0.15 g of white powder were dissolved in solvent of 5ml ethylenediamine and 10ml CH_3CN and 0.1 g catechol were dissolved into 20ml CH_3OH respectively, stirring at room temperature. After two hours, the above solution were mixed, then stirring for about 16h, the solution was filtrated, red filtrate was layered by Et2O for 1-3 weeks and under fluorescence microscope a light coral platy needler-shaped single crystal 1 (yield: 24%) and a red bulk crystal 2 (yield: 9%) was obtained. ^{1}HNMR (600 MHz, D_2O) crystal 1:δ 6.37 (d, 4H); δ 6.22 (t, 4H); δ 3.01-2.61 (m, 8H), crystal 2:δ 6.47 (d, 4H); δ 6.21 (d, 4H); δ 3.01-2.73(m, 8H). Calcd for $C_{17}H_{30}N_5O_6W$: 584.31; C, 34.94; H, 5.13; N, 11.98; O, 16.43. Found: C, 35.01; H, 5.61; N, 11.56; O, 16.33. Calcd for $C_{16}H_{26}N_4O_6W$: 554.26; C, 34.67; H, 4.69; N, 10.11; O, 17.32. Found: C, 34.71; H, 4.73; N, 10.23; O, 17.43. The IR data is shown in tableS1 and the IR spectra figures of the single crystals and their nano-objects are in supporting information figure S1, the UV-vis spectra and CV curve of the complex **1** and complex **2** which can be seen in supporting information (shown in figure S4) are quite similar.

Single-crystal structure determination by X-ray diffraction was performed on a Bruker Apex II CCD area detector device with Mo-Ka radiation. The structure was solved by direct methods with SHELXS-97.[41] An absorption correction based on symmetry equivalent reflections was applied using the SADABS program.[42] The final refinement included atomic positions for all of the atoms and anisotropic thermal parameters for all of the non-hydrogen atoms. Full-matrix least-squares structure refinement against |*F2*| was carried out with the SHELXTL-PLUS package of programs.[43]

Scheme 1. Coordination synthesis of complex and cultivation process of single crystals involved in this study

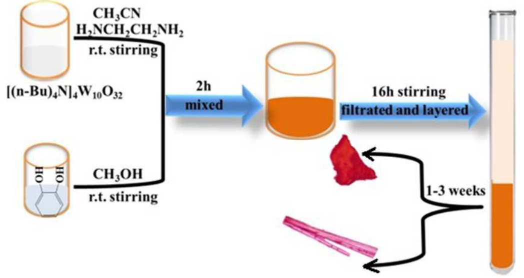

3. Preparation of nanostructures for complexes 1 and 2

The nanostructures were prepared by top-down method. The detailed process is as follows: First, we used ether to rinse single crystals which were obtained above; this is a very important step, the single crystal should be clean enough which means no solvent on the crystal surface or we can’t get powder but dope after artificial ground. To ensure the solvent on crystal surface volatilizes completely, the crystal is placed in a vacuum oven for 30mins with the temperature of 50~60℃。 Next, a small amount of clean crystals were put into an agate mortar and pulverized. Then adding an appropriate amount of ether and grinding continuously under room temperature until ether volatilized completely. Adding ether and grinding again, repeat the process until the golden yellow powder change into dark yellow, which needs about 2~3h. The color change was shown in supporting imformation figure S2 and the XRD of crystals and nanostructures are also in the supporting imformation (figure S3). Then, a small dose of this powder was put into a 10 ml centrifuge tube which containing 6ml of ether, then sonication treatment for 5 to 7h. Finally, a few drops of the suspension were disbursed on the carbon support membrane for TEM.

Result and discussion

Crystal Structures of complex 1 and 2

The selected bond Lengths and angles and hydrogen bonds of complexes 1 and 2 were shown in tableS2 and tableS3 and tableS4 in the supporting information. X-ray crystal structural analysis reveals that, the catechol as ligand banding with W^{VI} formed the complex anion $[(Cat)_2W^{VI}(O)_2]^{2-}$ (Figure 1A and 2A) respectively, then the tungsten complex anions combined with different protonated ethylenediamine cations, constituted two kinds of crystal. The complex 1 anion attracted by a half di-protonated ethylenediamine $(NH_3CH_2CH_2NH_3)^{2+}$, a mono-protonated ethylenediamine $(NH_3CH_2CH_2NH_2)^{+}$ and a non-protonated ethylenediamine $NH_2CH_2CH_2NH_2$ formed $(NH_3CH_2CH_2NH_3)_{0.5}(NH_3CH_2CH_2NH_2)[(Cat)_2W^{VI}(O)_2]\cdot(NH_2CH_2CH_2NH_2)$ (Figure 1B), with bond length 1.75±0.02 Å (W=O), 2.00±0.01 Å (W-O) and 2.12±0.01 Å (W-O). The crystal 1 in space group P2(1)/c with the cell parameter a=7.1077(6) Å, b=30.934(3) Å, c=9.8061(8) Å and β=102.769(2), which is similar to the crystal prepared in our previous work[40]. The crystal 3 we prepared before is a pale-yellow single crystal in space group P2(1)/c with cell parameter of a=7.1354(4) Å, b=30.778(2) Å, c=9.8145(5) Å. and β=102.696(2). In crystal lattice, the complex 1 anions parallel aligned along *a* and *c* axis (Figure 1C, 1D, 1F and 1G), and anti-parallel arranged along *b* axis (Figure 1E and 1H), attracted by cations $(NH_3CH_2CH_2NH_3)^{2+}$and $(NH_3CH_2CH_2NH_2)^{+}$, and formed the bulk crystal 1 together with non-protonated $(NH_3CH_2CH_2NH_2)$.

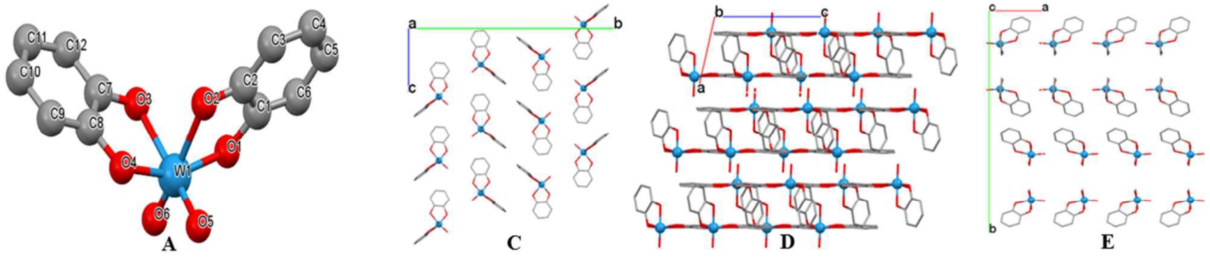

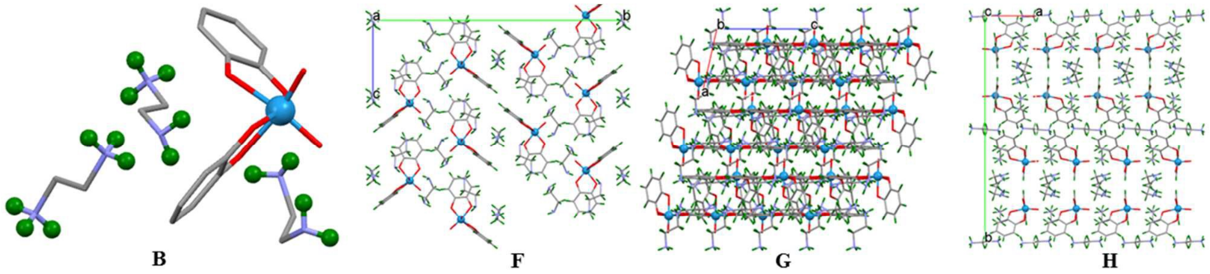

Figure 1 Molecular structure of complex 1 anion $[(Cat)_2W^{VI}(O)_2]^{2-}$ (A) and complex $(NH_3CH_2CH_2NH_3)_{0.5}(NH_3CH_2CH_2NH_2)[(Cat)_2W^{VI}(O)_2]\cdot(NH_2CH_2CH_2NH_2)$ (B). The packing of complex anion $[(Cat)_2W^{VI}(O)_2]^{2-}$ along *a* (C), *b* (D) and *c* (E) axis, the complex 1 along *a* (F), *b* (G), and *c* (H) axis, and the one-dimensional chainlike motif (D, G) and the H atoms are omitted for clarify except the H atoms linked with N atoms.

Table1. The related W=O and W-O lengths and O-W-O angles of two anions of complex2

Related bond	Bond lengths and angles					
W1 On	1.736	1.766	1.992	2.009	2.113	2.126
W2 On	1.752	1.777	1.990	2.001	2.095	2.139
O-W1-O	76.4	85.5	91.7	98.9	106.4	163.7
O-W2-O	75.9	84.1	91.2	101.7	105.3.3	165.7

Complex 2 anion attracted by two mono-protonated $(NH_3CH_2CH_2NH_2)^+$ structured $(NH_3CH_2CH_2NH_2)_2[(Cat)_2W^{VI}(O)_2]$ (Figure 2B). The crystal 2 in space group P2(1)/c with the cell parameter a=16.5081(7) Å, b=23.4259(8) Å, c=10.2617(3) Å, and β=92.433(3). In crystal lattice of complex 2, two different kinds of $[(Cat)_2W^{VI}(O)_2]^{2-}$ presented according to their bond lengths and angles, of which the W atoms are characterized by W1 and W2 respectively. The bond length and angle between W and O are list in table**1**. The complex anions parallel aligned along *b* and *c* axis (Figure 2C, 2D. 2F and 2G), and anti-parallel arranged along *a* axis (Figure 2E and 2H), attracted by cation $(NH_3CH_2CH_2NH_2)^+$, formed bulk crystal 2.

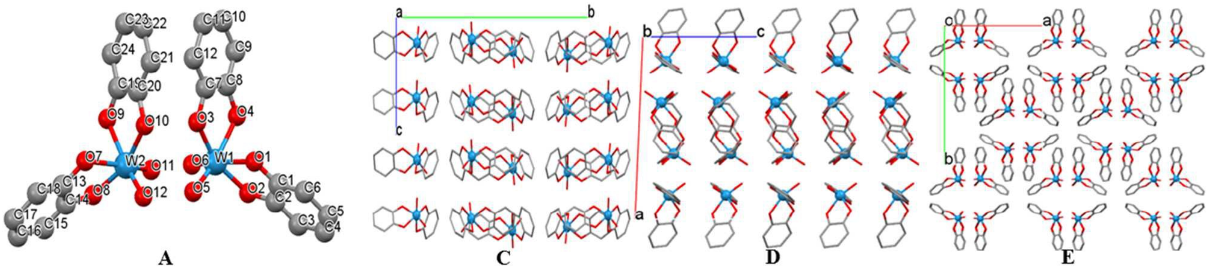

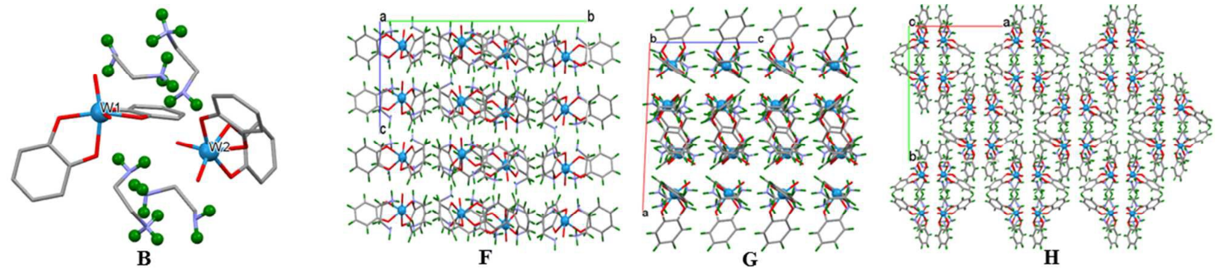

Figure 2 Molecular structure of complex2 anion $[(Cat)_2W^{VI}(O)_2]^{2-}$ (A) and complex $(NH_3CH_2CH_2NH_2)_2[(Cat)_2W^{VI}(O)_2]$ (B), the packing of the complex $(NH_3CH_2CH_2NH_2)_2[(Cat)_2W^{VI}(O)_2]$ along *a* (C), *b* (D) and *c* (E) axis, and complex2 anion along $[(Cat)_2W^{V}(O)_2]^{2-}$ along *a* (F), *b* (G) and *c* (H) axis, of which the H atoms are omitted for clarify except the H atoms linked with N atoms.

The complex 1 consisted of three different protonated ethylenediamine, i.e. a half di-protonated ethylenediamine $(NH_3CH_2CH_2NH_3)^{2+}$, a mono-protonated ethylenediamine $(NH_3CH_2CH_2NH_2)^+$, and a non-protonated $NH_2CH_2CH_2NH_2$ (Fig. 1B). However, complex 2 only possesses one kind of ethylenediamine, it is mono-protonated ethylenediamine $(NH_3CH_2CH_2NH_2)^+$ (Figure 2B). Because of the different chemical composition, two different W-based complexes packed in different mode in the crystal lattices. The repeating unit in crystal 1 is one-dimensional chain-like unit along *c* axis (Figure 1C, 1D, 1F and 1G). However, the repeating unit in crystal 2 is one-dimensional tubular-like motif along *c* axis (Figure 2C, 2D. 2F and 2G). Since the chain-like unit and tubular-like motif are linked by weak force (such as electrostatic attraction by $(NH_3CH_2CH_2NH_3)^{2+}$, $(NH_3CH_2CH_2NH_2)^+$ and $NH_2CH_2CH_2NH_2$, hydrogen bonds, and vander vaal forces) that is easy broken up. Therefore, under a suitable treatment, the two bulk crystals could disassemble into smaller aggregates such as in micro- and nano-scale. During the single crystal disassembly process, parts of the ethylenediamine evaporated, because of its volatileness.

Nanostructures prepared from bulk crystal 1 and 2

As deduced above, under scan electronic microscope (SEM) we have observed the W-directed micro-structures (Figure 3) which disassembled from crystal 1and 2 then re-assembled by complex 1and 2 after the bulk crystal ground into powder. Figure 3A exhibited that the bulk crystal 1 grinds into smaller parts and wires. Figure 3B and 3C presented the fine nanowires with diameter of 18-30 nm and lengths of micrometers, the nanowires are bundled or overlapped. Figure 3D and 3E indicated that the micro-tubules with diameter and lengths of 142-325 nm/ a few micrometres disintegrated from crystal 2. Figure 3F and 3G exhibited the sections of the tubules signed in white color. Figure 3H indicated that the tubule-like structure are fragile, which can be seen from the broken part signed by the circle in white color.

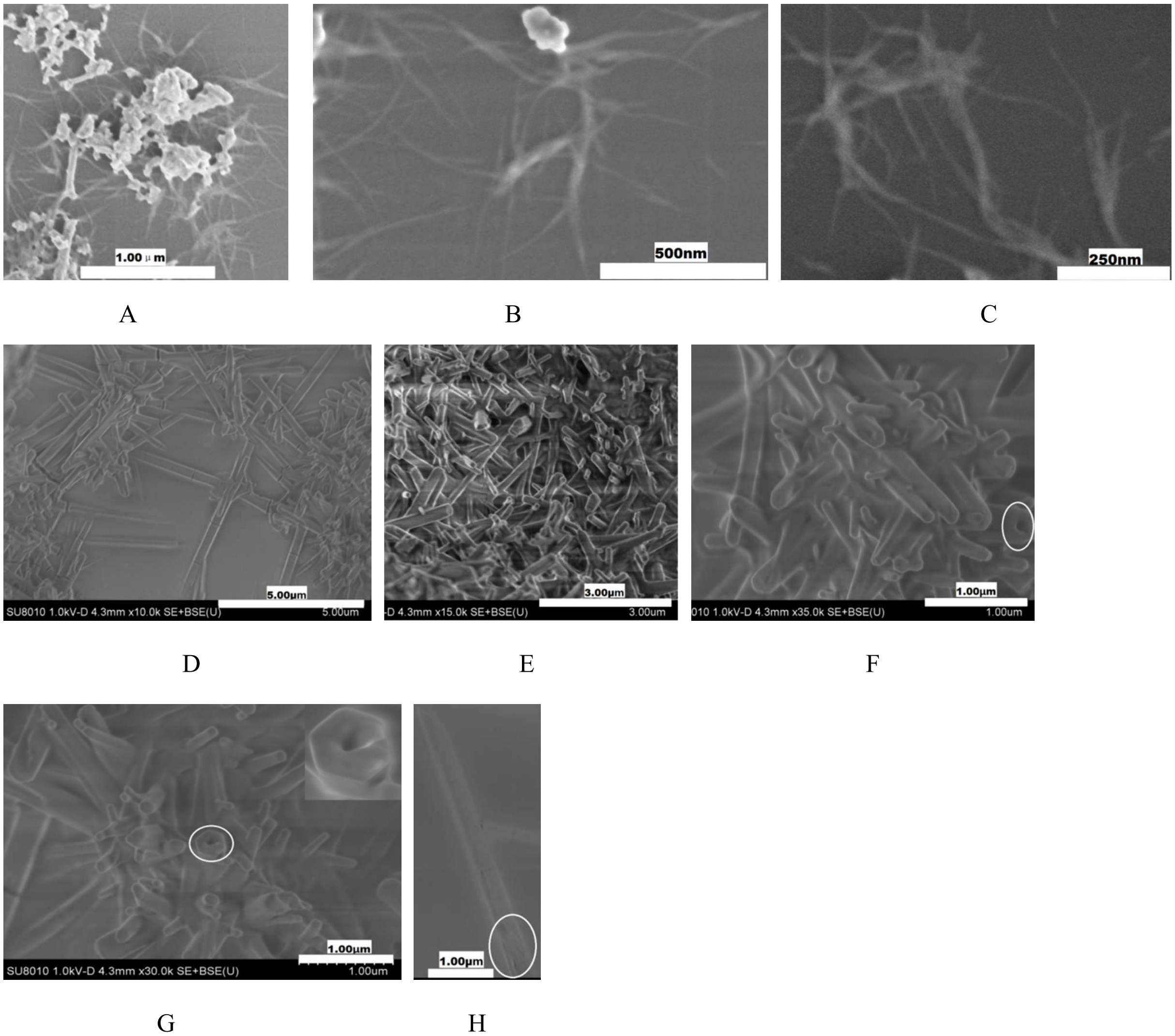

Figure 3 The SEM images of the micro-structure prepared from crystal 1 and 2. The broken parts and nanowires of complex 1 are exhibited in A. Nanowires with diameter of 18-30 nm and lengths of over micrometers (B and C). The needle-shaped crystal 2 are shown in D, from which the pseudo-micro-tubules curled by the bulge of the outer layer of the crystal can be seen clearly, Transformation of the surface of crystal 2 (E), almost superficial surface curled into nano-tubules with diameter of 142-325 nm and lengths of over micrometers. Nano-tubules are almost with uniform diameters (F and G), from which the hollows of the tubules and the fracture along radial direction exhibited obviously. The crack part of a nano-tubule (H) presented visibly.

Furthermore, taking advantage of the function of grinding and ultra-sonication we have fabricated the nano-architectures from the bulk crystal 1 and tubular crystal 2 respectively. The TEM images of the nanowire bundles prepared from crystal 1 were presented in figure 4A and 4B. Figure 4C is a thread of nanowire with diameter of 18 nm and length of over 1000 nm. Figure 4D is a bundle of nanowires, and near which a string of nano-particles can be seen. Figure 4E exhibited nanoparticles with pseudo-oval-morphologies with the size of a few nanometers. Figure 4A to 4E demonstrated that the bulk crystal 1 with quantum-wire motifs disassembled into nanowires which are similar to the wires shown in figure 3A to 3C, and then the nanowires broken down to pseudo-oval-nano-particles of a few nanometers. Moreover, crystal 2 with quantum-tubule motifs disassembled then reassembled into the nano-tubules which are analogous of the tubular structures shown in figure 3D to 3H. Figure 4F is a nano-tubule broken along radial direction, and figure 4G shown two nano-tubules which conked out at the tubule's tops, bottoms, and along the radial direction, which indicated that the nano-tubules of complex2 are fragile. Figure 4H and 4I not only show the nano-tubules are breakable further, but also presented some nanoparticles with almost uniform size. Figure 4J gave the detailed images of small plate-like particles with a few nanometers, which might be the smallest scale of the nano-species disassembled from crystal 2. From figure 4F to 4J, we deduced that under the treatment of grinding, the crystal 2 with multi-layered structure disassembled into micro-lamellas, then curled into macro-tubules. Furthermore, crystal 2 disassembled into nano-lamellas, and curled into nano-tubules through grinding and ultra-sonication.

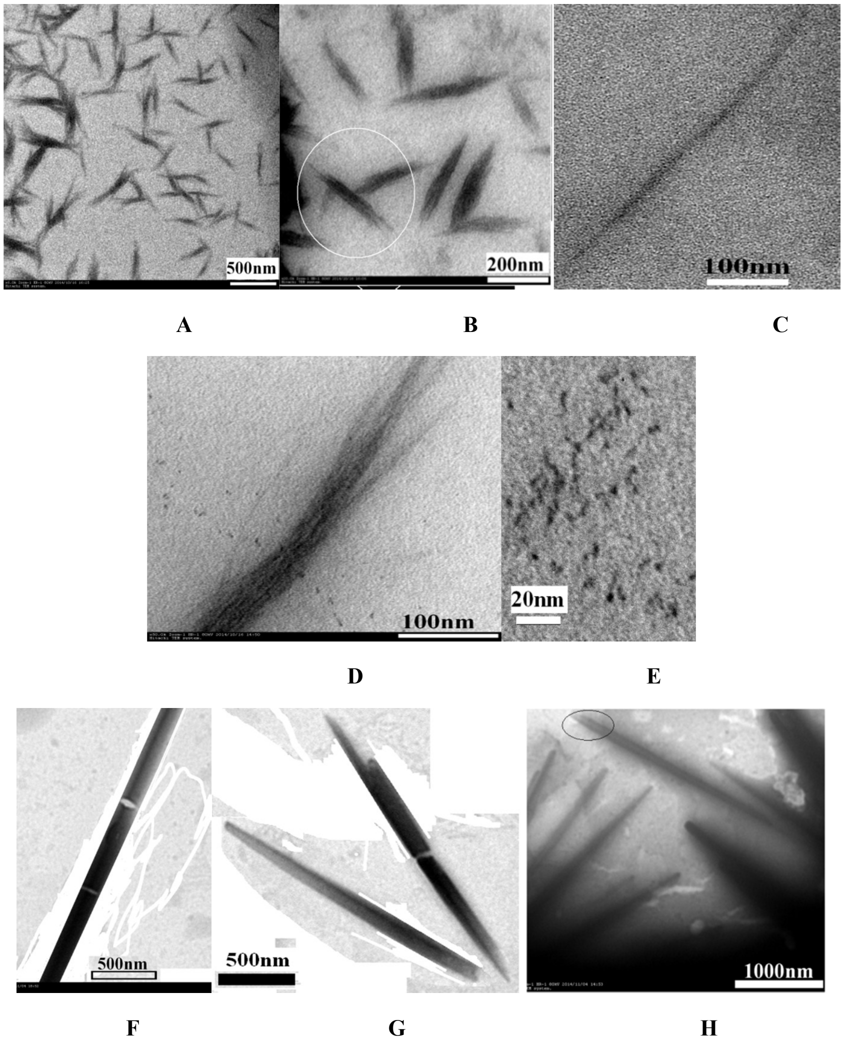

A B C

D E

F G H

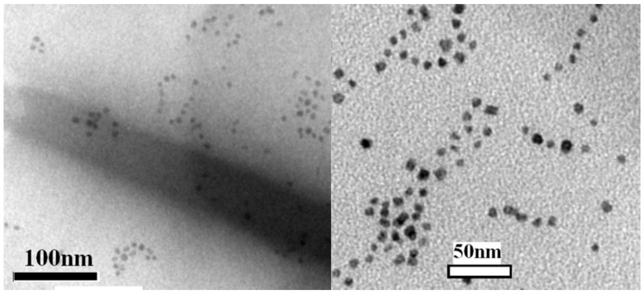

I J

Figure 4 TEM images of the nanostructures prepared from bulk crystal 1 and tubular crystal 2. Figure 4A to 4E correspond to crystal 1 and figure 4F to 4J correspond to crystal 2. Bundles of nanowires prepared from the bulk crystal 1 (A and B). A thread of nanowire with diameter of a few nanometers and lengths of hundreds nanometers located individually (C). A bundle of nanowires with diameter of a few nanometers and lengths of hundreds nanometers is displayed, the threads of nanowires, also a string nanoparticles, can be seen clearly (D). Pseudo-oval-like nanoparticles with the size of 1-4 nm displayed (E). A few nano-tubules with diameter of 50-75 nm and lengths over 2000 nm are presented (F). Two broken nano-tubules are busted at the top and bottoms and along the radial direction (G). A broken nano-tubule conked out along the radial direction (H). The broken nano-tubule signed by a circled in H, near which nanoparticles can be seen (I). And the pseudo-square-like nanoparticles in a few nanometer scale (J).

Comparisons of the PXRD of the Bulk Crystals with Their Associated Nanostructures.

To confirm the purities of the crystals, the PXRD spectra of the crystals are detected, shown in Figure S3. The experimental and simulated powder X-ray diffraction patterns are almost the same for the crystal 1 and crystal 2, respectively, which illustrated that the crystals 1 and 2 are pure. Furthermore, the PXRD spectra of nanostructures were determined (Figure S3), which are similar to those of their related bulk crystals except that the widths of the peaks are widened and the baselines are not level and smooth, which are due to that the crystallization in nanostructures is less than that in crystals. The same PXRD results of the nanostructures with bulk crystals illustrated that the chemical composition and the linkages among the chemical component are the same in both crystal and nanoaggregate states.

The formation Mechanism of the nanostructures

The two complexes in different shape and color consisted of the same anion $[(cat)WO_2]^{2-}$, combined with different protonated ethylenediamine cations revealed that the cations play an important part in the formation of the single crystals. And the protonated ethylenediamine cations also have an important influence on the micro- and nanostructures manufactured from the crystals. For clarify, the space filling model is used to describe the typical repeating unit of crystal 1 shown in figure 5A. Figure 5B and 5C indicated that the quantum-chain along *a* axis, parallel aligned along *c* axis and anti-parallel arranged along *b* axis. However, in crystal 2, the distinctive motif is the tubules displayed in Figure 5D. The quantum-tubule along *c* axis, parallel piled along *a* and anti-parallel arranged along *c* axis shown in figure5E and 5F. Both of the repeating motifs are linked by the protonated ethylenediamine cations through electrostatic attractions and hydrogen bond interaction, and constructed the bulk crystal 1 and 2 respectively. The electrostatic attractions and hydrogen bond interaction are weak interaction that is easy to be broken, which means that the crystal 1 and 2 can disassemble into small pieces such as in nanostructures. Meanwhile, the morphologies and sizes of the nanostructures are determined by the quantum motifs, which suggest that the crystal 1 with chain-like motif disassembled into nanowires, and the crystal 2 with tubular repeating unit disaggregated into nano-tubules.

Table 2. The corresponding information of crystal 1,2 and 3

Classification			Crystal 1	Crystal 2	Crystal 3[40]
Similarities			$[(Cat)_2W^{VI}(O)_2]^{2-}$; P2(1)/c space group; the units are linked by weak force		
differences	cell parameters	a	7.1077(6) Å	16.5081(7) Å	7.1354(4) Å
		b	30.934(3) Å	23.4259(8) Å	30.778(2) Å
		c	9.8061(8) Å	10.2617(3) Å	9.8145(5) Å
		β	102.769(2)°	92.433(3)°	102.696(2)°
	Amine types		di-,mono-,and non-protonated ethylenediamine	mono-protonated ethylenediamine	mono- and non-protonated ethylenediamine
	repeating units		one-dimensional chain along c axis	one-dimensional tubular along c axis	two-dimensional lamellar in the ac plane

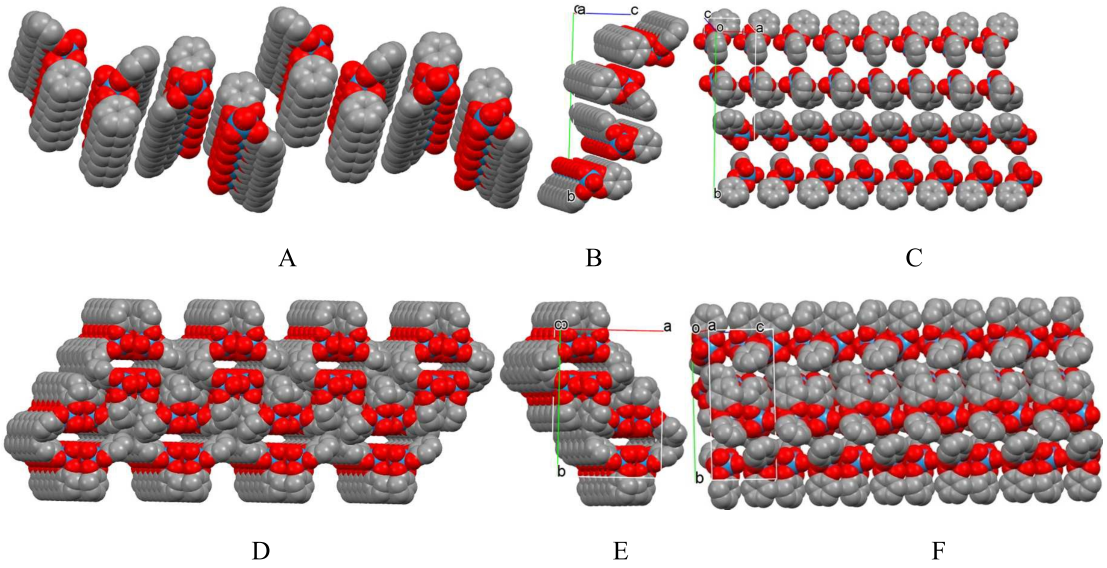

Figure 5 The packing of the W-based chain-like motif in crystal lattice 1 (A, B and C) and the stacking of the W-based tubular repeating unit in crystal 2 (D, E and F), of which all the ethylendiamine related molecules and the H atoms are omitted for clarify.

In addition, the complex $(NH_3CH_2CH_2NH_2)_2[(Cat)_2W^{VI}(O)_2]\cdot(NH_2CH_2CH_2NH_2)$ (3) (figure 6A)[40] which is the analogous of the complex $(NH_3CH_2CH_2NH_3)_{0.5}(NH_3CH_2CH_2NH_2)$ $[(Cat)_2W^V(O)_2]\cdot(NH_2CH_2CH_2NH_2)$ (1), and the two crystals possess the similar crystallographic parameters such as a, b c ,α, β, and γ. However, they produced the quite different nanostructure i.e. complex 3 produced multi-nano-pipes (figure 6B) but complex 1 produced nanowires. For more intuitive express the seminaries and differences between the three crystals, the corresponding information of crystal 1, 2 and 3 is presented in table 2.

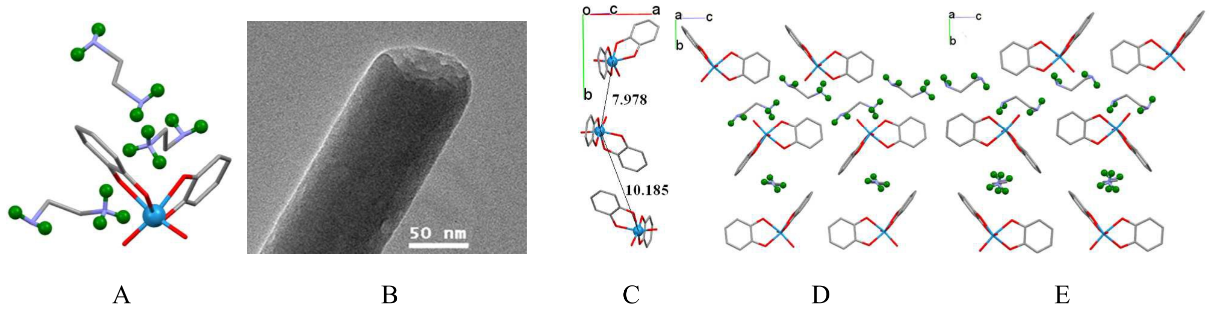

Figure 6 Molecular structure of $(NH_3CH_2CH_2NH_2)_2[(Cat)_2W^{VI}(O)_2]\cdot(NH_2CH_2CH_2NH_2)$ (A). Nano-pipes and their aggregated morphology of complex 3 (B). The distances of the gaps formed by neighboring chains along *b* axis (C). The mono-protonated cation $(NH_3CH_2CH_2NH_2)^+$ located at the smaller gap with distance of 7.798 Å and the neutral $NH_2CH_2CH_2NH_2$ positioned at the larger space with distances of 10.185 Å (D) in crystal lattice 3. The neutral $NH_2CH_2CH_2NH_2$ located at the smaller gap with distance of 7.798 Å and the bi-protonated cations $(NH_3CH_2CH_2NH_3)^{2+}$ positioned at the larger space with distances of 10.185 Å (D) in crystal lattice 1.

The formation mechanism of different nanostructures might originate in the cations located between the chains with different distance. As shown in figure 6C, the gaps between the adjacent chains can be divided into smaller gap and larger gap with distance 7.798 Å and 10.185 Å respectively, along *b* axis. In crystal lattice 3, the mono-protonated $(NH_3CH_2CH_2NH_2)^+$ located at the smaller gaps, and the neutral molecule $NH_2CH_2CH_2NH_2$ positioned at the large gaps. However, in crystal lattice 1, the neutral molecule $NH_2CH_2CH_2NH_2$ located at the smaller gaps and the bi-protonated $(NH_3CH_2CH_2NH_3)^{2+}$ positioned at the larger gaps. Obviously, the electrostatic attraction is as follows: $(NH_3CH_2CH_2NH_3)^{2+} > (NH_3CH_2CH_2NH_2)^+ > NH_2CH_2CH_2NH_2$, therefore, the linkages in the smaller gaps is stronger than that in the larger gaps for crystal 3, whereas, inverse for crystal 1. Then the bulk crystal 3 is easier to crack at the larger space with the distance of 10.185 Å, and then disassembled into nano-ribbons which curled into nano-pipes and bundled together. In contrast, crystal 1 with the multi-chains are difficult to break up from the larger gaps, since the neighboring chains are linked by $(NH_3CH_2CH_2NH_3)^{2+}$ that the electrostatic attraction is much stronger than the neutral $NH_2CH_2CH_2NH_2$ located at smaller gaps, hence crystal 1 split into nanowires, rather than nano-ribbon or nano-pipes.

Conclusion

A pair of W-directed coordination architectures $(NH_3CH_2CH_2NH_3)_{0.5}(NH_3CH_2CH_2NH_2)[(Cat)_2W^{VI}(O)_2]\cdot(NH_2CH_2CH_2NH_2)$ (1) and $(NH_3CH_2CH_2NH_2)_2[(Cat)_2W^{VI}(O)_2]$ (2) was successfully synthesized by wet method, and bulk single crystal **1** with $[(Cat)_2W^{VI}(O)_2]^{2-}$-based quantum-wire motifs and crystal **2** with $[(Cat)_2W^{VI}(O)_2]^{2-}$-based quantum-tubule motifs were obtained. By grinding and ultra-sonication, crystal**1** disintegrated into nanowires with diameter about 18nm and lengths of hundreds nanometers, and crystal **2** disassembled into nano-tubules with diameter and length of 15-18nm/ 450-550nm. The quantum chains induced the formation of the nanowires and the quantum tubules led to the production of the nano-tubules. Compared with the multi-pipes prepared from the W-based amorphous in previous work. It indicated that, located at the same gaps with the same distance between the $[(Cat)_2W^{VI}(O)_2]^{2-}$-based quantum chains, $(NH_3CH_2CH_2NH_3)^{2+}$ attracted the chains stronger than neutral $NH_2CH_2CH_2NH_2$, hence crystal **1** split into nanowires, while W^{VI}-based crystal **3** cracked into regular nano-ribbon then curled into uniform nano-pipes bundled together. This article studied the influence of protonated degree Ethylenediamine on the formation of $[(Cat)_2W^{VI}(O)_2]^{2-}$-directed macro-, micro and nano-architectures. The distinguished results indicated that a slight adjustment of ethylenediamine protonated degree can induced a great transformation of micro- and nano-architectures' morphologies and scale. The result also offered a new method to assemble quite different nanostructures, only by changing the protonation degree of the multi-amine.

* **Supporting Information**

CIF files. This material is available free of charge via the Internet at http://pubs.rsc.org.

AUTHOR INFORMATION

Corresponding Author

*E-mail: lu-xiaoming@126.com.

Notes

The authors declare no competing financial interest.

ACKNOWLEDGMENTS

We gratefully acknowledge financial support from the Natural National Science Foundation (granted No. 21173150) and the foundation of Fujian Institute of Research on the structure of Matter, Chinese Academy (granted No. 20130007).

Reference

1 R. Tenne, L. Margulis, M. Genut and G. Hodes, Nature, 1992, 360,444.
2 A. A. Ashkarran, A. I. Zad, M. M. Ahadian and S. A. M. Ardakani, Nanotechnology, 2008, 19, 195709.
3 Z.-G. Zhao and M. Miyauchi, Angew. Chem., Int. Ed., 2008, 47, 7051.
4 R. Abe, H. Takami, N. Murakami and B. Ohtani, J. Am. Chem. Soc., 2008, 130, 7780.
5 Y. Y. Liu, J. Yu, H. Huang, B. H. Xu, X. L. Liu, Y. Gao and X. L. Dong, Surf. Coat. Technol., 2007, 201, 7246.

6 S. F. Abdullah, S. Radiman, M. Azmi, A. Hamid and N. B. y. Ibrahim, Sains Malays., 2008, 37, 227.

7 J. Wu, W. Zhai and G. Jie, Tribol. Int., 2010, 43, 1650.

8 L. Wang, A. Teleki, S. E. Pratsinis and P. I. Gouma, Chem. Mater., 2008, 20, 4794.

9 T. Kida, A. Nishiyama, M. Yuasa, K. Shimanoe and N. Yamazoe, Sens. Actuators, B, 2009, 135, 568.

10 Y. Zhao, J. He, M. Yang, S. Gao, G. Zuo, C. Yan and Z. Cheng, Anal. Chim. Acta, 2009, 654, 120.

11 R. Ganesan and A. Gedanken, Nanotechnology, 2008, 19, 025702.

12 T. H. Nguyen, T. V. Nguyen, C. G. Cooper and A. A. Adesina, Stud. Surf. Sci. Catal., 2006, 159, 781.

13 M. Lei, H. Z. Zhao, H. Yang, B. Song, L. Z. Cao, P. G. Li and W. H. Tang, J. Alloys Compd., 2008, 460, 130.

14 P. G. Li, M. Lei and W. H. Tang, Mater. Res. Bull., 2008, 43, 3621.

15 A. H. Mahan, P. A. Parilla, K. M. Jones and A. C. Dillon, Chem. Phys. Lett., 2005, 413, 88.

16 U. Qureshi, C. Blackman, G. Hyett and I. P. Parkin, Eur. J. Inorg. Chem., 2007, 1415.

17 V. L. Goncharov, Y. V. Lakhotkin, V. P. Kuzmin, V. K. Alimov and J. Roth, Adv. Mater. Res., 2009, 59, 62.

18 H. H. Nersisyan, H. I. Won, C. W. Won and K. C. Cho, Powder Technol., 2009, 189, 422.

19 H. I. Won, H. H. Nersisyan and C. W. Won, J. Nanopart. Res., 2010, 12, 493.

20 T. Rodriguez-Suarez, L. A. Diaz, S. Lopez-Esteban, C. Pecharroman, A. Esteban-Cubillo, L. Gremillard, R. Torrecillas and J. S. Moya, Nanotechnology, 2008, 19, 215605.

21 M. Zhu, L. Y. Dai, N. S. Gu, B. Cao and L. Z. Ouyang, J. Alloys Compd., 2009, 478, 624.

22 N. Asim, S. Radiman and M. A. Bin Yarmo, Mater. Lett., 2007, 61, 2652.

23 E. Reverchon, G. Della Porta and E. Torino, J. Supercrit. Fluids, 2010, 53, 95.

24 K. Essaki, E. J. Rees and G. T. Burstein, J. Am. Ceram. Soc., 2010, 93, 692.

25 N. Le Houx, G. Pourroy, F. Camerel, M. Comet and D. Spitzer, J. Phys. Chem. C, 2010, 114, 155.

26 C. Vollmer, E. Redel, K. Abu-Shandi, R. Thomann, H. Manyar, C. Hardacre and C. Janiak, Chem.–Eur. J., 2010, 16, 3849.

27 M. Leparoux, C. Schreuders, J.-W. Shin and S. Siegmann, Adv. Eng. Mater., 2005, 7, 349.

28 T. Ryu, H. Y. Sohn, K. S. Hwang and Z. Z. Fang, J. Mater. Sci., 2008, 43, 5185.

29 T. Ryu, H. Y. Sohn, K. S. Hwang and Z. Z. Fang, J. Am. Ceram. Soc., 2009, 92, 655.

30 S. Supothina, P. Seeharaj, S. Yoriya and M. Sriyudthsak, Ceram. Int., 2007, 33, 931.

31 B. A. Hernandez-Sanchez, T. J. Boyle, H. D. Pratt, III, M. A. Rodriguez, L. N. Brewer and D. R. Dunphy, Chem. Mater., 2008, 20, 6643.

32 B. Zhang; S. Z. Du; X. M. Lu; G. Wang and J. Fen. Inorg.Chem. 2013, 52, 9470−9478.

33 B. Zhang; X. M. Lu; K. Li; S. Z. Du; G. Wang and Q. Wang. Cryst.Growth Des.2014, 14, 3249−3256.

34 Zixiang Chi; Linli Zhu; Xiaoming Lu; Hongtao Yu and Bing Liu. Z. Anorg. Allg.Chem. 2012, 638, (10), 1523–1530.

35 Shi-Zhen Du; Jun Feng; Yi-Feng Cheng; Lan An and Xiao-Ming Lu. Z. Anorg. Allg. Chem. 2012, 638, (2), 411–414.

36 Yu Chong; Shi Xudong; Chi Zixiang; Bi Yangang; ChenYuyou ; Ye Chaohui & Lu Xiaoming. Journal of Coordination Chemistry. Vol. 64, No. 14, 20 July 2011, 2521–2530.

37 Zixiang Chi; Linli Zhu; Yuyou Chen; Chong Yu; Xudong Shi; Yangang Bi; and Xiaoming Lu. Z. Anorg.Allg. Chem. 2011, 637, 436–440.

38 X.M. Lu; X.D. Shi; Y.G. Bi; Z.X. Chi; T. Min; L.L. Zhu; S.F. Xiao; L.J. Zhong. ApplPhys A (2011) 103: 551–554.

39 Xiaoming Lu; Xudong Shi; and Tao Min. Inorg. Chem. 2011, 50, 2175–2181.

40 Du Shizhen; Lu Xiaoming; Feng Jun; Cheng Yifeng; AnLan and Sun Xiaojing.CrystEngComm,2012, 14, 6618–6626.

41 G. M. Sheldrick, SHELXTL-97 V5.10, Bruker AXS Inc., Madison, WI, 1997.

42 G. M. Sheldrick, SADABS, Program for Empirical Absorption Correction of Area Detector Data, University of Gottingen, Gottingen, 1996.

43 G. M. Sheldrick, SHELXTL-PLUS, Siemens Analytical X-ray Instruments Inc., Madison, WI, 1990.

Effects of ethylenediamine in the formation of macro-, micro, and nano- structures based on $[W^{VI}(Cat)_2O_2]^{2-}$

Ganghuo Pan[a] Xiaoming Lu*[ab] Kai Li[a] Minghai Shen[a] Jing Zhao[a]

Department of Chemistry, Capital Normal University, China, Beijing 100048

b State Key Laboratory of Structural Chemistry, Fujian Institute of Research on the Structure of Matter, Chinese Academy of Sciences, Fuzhou, Fujian 350002, China.

E-mail: lu-xiaoming@126.com

Only For Graphical Table of Contents

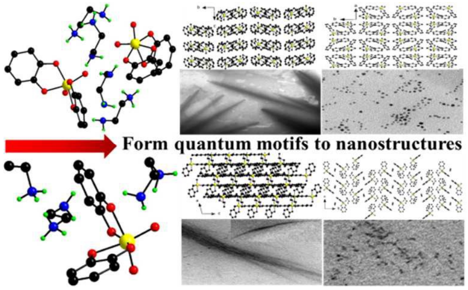

A slight change in the protonation of ethylenediamine affects the nanostructure greatly during the crystals formation